Article

Peroxynitrite Activatable NIR-II Fluorescent Molecular Probe for Drug-induced Hepatotoxicity Monitoring

Dandan Li, Shangfeng Wang, Zuhai Lei, Caixia Sun, Ahmed Mohamed El-Toni, Mansour Saleh Alhoshan, Yong Fan, and Fan Zhang

Anal. Chem., **Just Accepted Manuscript** • DOI: 10.1021/acs.analchem.9b00317 • Publication Date (Web): 27 Feb 2019

Peroxynitrite Activatable NIR-II Fluorescent Molecular Probe for Drug-induced Hepatotoxicity Monitoring

Dandan Li[1], Shangfeng Wang[1], Zuhai Lei[1], Caixia Sun[1], Ahmed Mohamed El-Toni[2], Mansour Saleh Alhoshan[3], Yong Fan[1], Fan Zhang[1]*

1. Department of Chemistry, Shanghai Key Laboratory of Molecular Catalysis and Innovative Materials, State Key Laboratory of Molecular Engineering of Polymers and iChem, Fudan University, Shanghai 200433, P. R. China.

2. King Abdullah Institute for Nanotechnology, King Saud University, Riyadh 11451, Saudi Arabia.

3. Department of Chemical Engineering, King Saud University, Riyadh 11421, Saudi Arabia.

Tel: (+86)21-51630322; Fax: (+86)21-5163-0307

E-mail: zhang_fan@fudan.edu.cn.

ABSTRACT

Drug-induced hepatotoxicity represents an important challenge for safety in drug development. The production of peroxynitrite ($ONOO^-$) is proposed as an early sign in the progression of drug-induced hepatotoxicity. Currently, reported $ONOO^-$ probes mainly emit in visible range or the first NIR window, which have limited in vivo biosensing application due to the autofluorescence and photon scattering. Herein, we developed a peroxynitrite activatable second near-infrared window (NIR-II) molecular probe for drug-induced hepatotoxicity monitoring, based on the fusion of an NIR-II fluorescence turn-on benzothiopyrylium cyanines skeleton and the phenyl borate. In the presence of $ONOO^-$, the probe IRBTP-B can turn on its NIR-II fluorescence by yielding its fluorophore IRBTP-O and display good linear response to $ONOO^-$. Tissue phantom study confirmed reliable activated signals could be acquired at a penetration depth up to 5 mm. Using this probe, we disclose the upregulation of $ONOO^-$ in preclinical drug-induced liver injury model and the remediation with N-acetyl cysteine (NAC) in vivo. We expect that this strategy will serve as a general method for the development of activatable NIR-II probe based on the hydroxyl functionalized reactive sites by analyte-specific triggering.

KEYWORDS

NIR-II probe, fluorescence, activatable, peroxynitrite, hepatotoxicity

INTRODUCTION

Drug toxicity is not only an important safety evaluation target in preclinical research and development of candidate drugs, but also a major cause for post-marketing drug withdrawals.[1] Metabolic organs, especially liver, are the major site to convert drugs to various metabolites.[2] In the liver, drugs are enzymatically biotransformed into polar, water-soluble, and excretable metabolites accompanied by the generation of reactive radicals or reactive electrophiles, such as reactive oxygen species (ROS) and reactive nitrogen species (RNS), to affect normal liver physiology, which is the

primary cause of drug-induced hepatotoxicity.[3,4] The production of RNS, particularly peroxynitrite ($ONOO^-$), is proposed as an early sign in the progression of drug-induced hepatotoxicity.[5]

For the $ONOO^-$ detection, fluorescence imaging is a promising tool owing to the advantages of being non-invasive, good sensitivity and selectivity.[6-9] Up to now, quite a few fluorescence probes for $ONOO^-$ detection in visible range and the first near-infrared window (NIR-I, 750-900 nm) were reported.[10-25] However, the fundamental barriers to bio-tissue fluorescence imaging in those windows is the photon penetration depth which is limited by the wavelength-dependent behavior of scattering and absorption.[26] Recently, fluorescence imaging in the second near-infrared window (NIR-II, 900-1700 nm) has come into the spotlight because it can benefit from the reduced autofluorescence, absorption and scattering to reach deeper penetration depths, resulting in high image quality and diffraction-limited resolution.[27-30] Till now, the majority of NIR-II contrast agents for in vivo imaging are comprised of nanomaterials such as carbon-nanotube[31], quantum-dot[32] and rare-earth doped nanoparticles[33,34]. Owing to unknown long-term toxicity concerns, it is necessary to design organic small-molecule NIR-II fluorophores to facilitate FDA approval and clinical translation. So far, there are only a handful of organic molecules with fluorescence NIR-II emission.[35-42] However, an intrinsic issue of above NIR-II contrast agents is their always-on fluorescence behavior, which means that the fluorescent signals have no response to specific target. This is one of the primary reasons for hampering the in vivo biosensing applications[43,44].

Herein we developed $ONOO^-$ activatable NIR-II fluorescent probe (IRBTP-B) based on the incorporation of phenyl borate group and benzothiopyrylium cyanines skeleton. In the presence of $ONOO^-$, the masking group phenyl borate can be removed to turn on the NIR-II fluorescence. Tissue phantom study confirmed reliable activatable signal was acquired at a penetration depth up to 5 mm. Using an acetaminophen (APAP)-induced liver injury model, we successfully realized the real-time monitoring of preclinical drug-induced liver injury.

EXPERIMENTAL SECTION

Synthesis of 7-bromo-2-(4-methoxyphenyl)-4H-thiochromen-4-one (1). A mixture of polyphosphoric acid (PPA, 22 g), 3-bromothiophenol (2 g, 10.6 mmol) and ethyl 3-(4-methoxyphenyl)-3-oxopropanoate (2.6 g, 11.66 mmol) was stirred at 95 ^{o}C for 2 h. After cooling to room temperature, ice water was added to quench the reaction and extracted with DCM (100 mL × 3). The combined organic extracts were dried with Na_2SO_4, filtered, and evaporated. The crude product was further purified by a flash column chromatography [silica gel, PE/DCM = 1/1 to 0/1, v/v] to give **1** (yield: 2.6 g , 70%). ^{1}H NMR (400 MHz, $CDCl_3$) δ 8.53 (d, *J* = 8.0 Hz, 1H), 7.86 (d, *J* = 8.0 Hz, 1H), 7.69 (d, *J* = 8.0 Hz, 2H), 7.43 (t, *J* = 8.0 Hz, 1H), 7.24 (d, *J* = 16.0 Hz, 1H), 7.02 (d, *J* = 8.0 Hz, 2H), 3.88 (s, 3H).

Synthesis of 7-(diethylamino)-2-(4-methoxyphenyl)-4H-thiochromen-4-one (2). A tube was charged with compound **1** (694 mg, 2 mmol), $Pd_2(dba)_3$ (45.8 mg, 0.05 mmol), DavePhos (19.7 mg, 0.05 mmol), and Cs_2CO_3 (1.63 g, 5 mmol, 5 mmol). The tube was sealed and evacuated/backfilled with nitrogen (3×). Anhydrous dioxane (10 mL) was added, following the addition of dibutylamine (1.7 mL, 10 mmol). The reaction was stirred at 100 °C for 18 h. After cooling to room temperature, the mixture was filtered, and the filtrate was evaporated. The crude product was further purified by silica gel column chromatography (EA/DCM = 1/10, v/v), obtaining product **2** (685 mg, 86.6 %).^{1}H NMR (400 MHz, $CDCl_3$): δ 8.32 (d, J=12 Hz, 1H),7.62 (d, J=12 Hz, 2H), 7.09 (s, 1H), 6.98 (d, J=12 Hz, 2H), 6.84-6.81 (dd, J_1=4 Hz, J_2=12 Hz, 1H), 6.64 (s, 1H), 3.87 (s, 3H), 3.36 (t, J=8 Hz,4H), 1.65-1.58 (m, 4H), 1.44-1.35 (m, 4H), 0.99 (t, J=8 Hz, 6H). ^{13}C NMR (100 MHz, $CDCl_3$): δ 180.0, 161.4, 150.5, 149.9, 140.3, 129.8, 129.2, 128.1, 121.8, 119.4, 114.4, 112.9, 104.8, 55.4, 50.7, 29.2, 20.2, 13.9. Maldi-Tof/Tof-MS: calcd for $C_{20}H_{22}NO_2SH^+$ $[M+H]^+$, 396.1992; Found, 396.3009. $[M+H]^+$..

Synthesis of 7-(diethylamino)-2-(4-methoxyphenyl)-4-methylthiochromenylium perchlorate (3). Compound **2** (395 mg, 1 mmol) was dissolved in anhydrous THF (10 mL) in a flame dried flask

under nitrogen. 1.0 M CH_3MgBr (3.6 mL) was added dropwise to this solution and allowed to stir at room temperature for 2 h. The solution was poured into 10% aqueous $HClO_4$ (10 mL) and extracted with DCM (25 mL × 3). The combined organic extracts were dried with Na_2SO_4, filtered, and evaporated to give **3** (yield: 480 mg, 97.3 %) without further purification. ^{1}H NMR (400 MHz, $CDCl_3$) δ 8.27 (d, *J* = 8Hz, 1H), 7.91 (s, 3H), 7.38 (d, *J* = 8Hz, 1H), 7.32 (s, 1H), 6.99 (d, *J* = 8Hz, 2H), 3.84 (s, 3H), 3.55 (s, 4H), 2.90 (s, 3H), 1.67 (s, 4H), 1.46 (s, 4H), 1.00 (s, 6H); ^{13}C NMR (100 MHz, $CDCl_3$) δ 164.1, 162.8, 159.9, 151.8, 145.5, 132.0, 129.7, 126.5, 124.4, 121.5, 119.6, 115.5, 105.8, 55.8, 51.7, 29.3, 23.0, 20.0, 13.8; Maldi-Tof/Tof-MS: calcd for $C_{25}H_{32}NOS^+$ $[M]^+$, 394.2199; Found, 394.2234. $[M]^+$.

Synthesis of IRBTP-O. A mixture of 4-hydroxyisophthalaldehyde (50 mg, 0.33 mmol) and compound 3 (329 mg, 0.66 mmol) was dissolved in Toluene/n-butanol (3 mL/3 mL). The reaction mixture stirred for overnight at 100 °C under an Ar atmosphere. After completion, the reaction mixture was concentrated by evaporation under reduced pressure. The crude product was purified by preparative RP-TLC (DCM/MeOH = 10:1, v/v) to give the desired product (yield: 105 mg, 35%). ^{1}H NMR (400 MHz, DMSO-d_6) δ 8.97-8.76 (m, 2H), 8.66-8.17 (m, 5H), 8.05 (t, J = 8Hz, 2H), 7.95-7.55 (m, 4H), 7.45-7.32 (m, 2H), 7.27-7.10 (m, 5H), 6.97-6.81 (m, 1H), 6.57 (d, J = 8 Hz, 1H), 6.50 (d, J = 8 Hz, 1H), 3.89 (s, 3H), 3.83 (q, J = 8 Hz, 2H), 3.74-3.67 (m, 2H), 3.62 (s, 2H), 3.53 (s, 2H), 3.19 (s, 3H), 1.60 (s, 4H), 1.41-1.19 (m, 12H), 0.93 (q, J = 8 Hz, 8H), 0.87 (t, J = 8 Hz, 4H). ^{13}C NMR (100 MHz, DMSO-d_6) δ 164.0, 163.6, 159.9, 158.2, 158.0, 154.3, 154.2, 152.0, 147.3, 145.6, 145.3, 145.0, 134.1, 132.3, 132.2, 130.00, 127.7, 126.9, 119.4, 119.2, 119.1, 118.7, 118.5, 115.9, 115.8, 114.20, 107.2, 56.3, 55.5, 50.9, 50.0, 29.4, 20.1, 19.9, 14.2. HRMS (ESI) m/z calcd for $C_{58}H_{65}N_2O_3S_2^+$ $[M]^+$, 901.4431; Found, 901.4459.

Synthesis of 2-(4-(iodomethyl)phenyl)-4,4,5,5-tetramethyl-1,3,2-dioxaborolane (4). (4-(4,4,5,5-tetramethyl-1,3,2-dioxaborolan-2-yl)phenyl)methanol (2 g, 8.5 mmol) was dissolved in 60

mL acetonitrile and cooled to 0 °C. NaI (3.84 g, 25.63 mmol) was added, and then TMSCl (3.25 mL, 25.63 mmol) was added dropwise. The reaction mixture stirred for 30 mins at room temperature, then diluted with EtOAc, and washed with water, then brine, dried over Na_2SO_4, and evaporated under reduced pressure. The crude product was purified by column chromatography on silica gel (EtOAc/PE = 5:95, v/v) to give compound 4 as a white solid (yield:2.44 g, 83 %). ^{1}H NMR (400 MHz, $CDCl_3$) δ7.75 (d, *J* = 6Hz, 2H), 7.40 (d, *J* = 6Hz, 2H), 4.46 (s, 2H), 1.35 (s, 12H).

Synthesis of Compound 5. 4-hydroxyisophthalaldehyde (200 mg, 1.33 mmol) was dissolved in 4 mL dry DMF and cooled to 0 °C. K_2CO_3 (405 mg, 2.93 mmol) was added and the solution stirred at 0 °C for 10 min. Then compound 4 (916 mg, 2.66 mmol) was added. The reaction mixture stirred at room temperature for 12h. After completion, the reaction mixture diluted with Et_2O and was washed with saturated solution of NH_4Cl. The organic layer was separated, washed with brine, dried over Na_2SO_4, and evaporated under reduced pressure. The crude product was purified by column chromatography on silica gel (EA/PE = 3:7, v/v) to give compound 5 (yield: 380 mg, 78%). ^{1}H NMR (400 MHz, $CDCl_3$) δ10.56 (s, 1H), 9.94 (s, 1H), 8.36 (d, *J* = 2Hz, 1H), 8.08 (dd, J_1 = 2Hz, J_2 = 8Hz, 1H), 7.87 (d, *J* = 8Hz, 2H), 7.45 (d, *J* = 8Hz, 2H), 7.18 (d, *J* = 8Hz, 1H), 5.32 (s, 1H), 1.35 (s, 12H). ^{13}C NMR (100 MHz, $CDCl_3$) δ 190.4, 188.7, 165.1, 138.1, 135.7, 135.6, 132.1, 130.0, 126.7, 125.4, 113.9, 84.2, 71.2, 25.1.

Synthesis of IRBTP-B. A mixture of compound 5 (100 mg, 0.27 mmol) and compound 3 (269 mg, 0.54 mmol) was dissolved in Toluene/n-butanol (3 mL/3 mL). The reaction mixture stirred for overnight at 100 °C under an Ar atmosphere. After completion, the reaction mixture was concentrated by evaporation under reduced pressure. The crude product was purified by preparative RP-TLC (DCM/MeOH = 10:1, v/v) to give the desired product (yield: 98 mg, 32%). ^{1}H NMR (400 MHz, DMSO-d_6) δ9.08 (d, J = 8Hz, 1H), 8.88 (s, 1H), 8.80 (d, J = 8Hz, 1H), 8.46 (d, J = 16Hz, 1H), 8.28 (s, 3H), 8.20 (d, J = 16Hz, 1H), 8.06 (d, J = 8Hz, 3H), 8.02 (d, J = 8Hz, 1H), 7.90 (d, J = 8Hz, 2H),

7.80 (d, J = 8Hz, 2H), 7.60 (d, J = 8Hz, 2H), 7.51 (s, 1H), 7.46 (s, 1H), 7.25-7.15 (m, 7H), 5.28 (s, 2H), 3.90 (d, J = 8Hz, 6H), 3.35 (s, 8H), 1.50 (s, 8H), 1.34 (s, 18H), 1.22 (s, 2H), 0.92 (s, 12H). ^{13}C NMR (100 MHz, DMSO-*d*6) δ 163.7, 163.5, 159.8, 158.2, 157.6, 153.9, 153.5, 151.7, 145.5, 145.3, 144.5, 140.0, 135.2, 133.0, 132.7, 129.9, 129.6, 127.4, 127.3, 125.0, 122.3, 119.4, 119.2, 119.1, 118.9, 118.0, 115.9, 115.8, 113.9, 107.0, 106.9, 84.3, 70.6, 56.3, 50.8, 29.5, 25.4, 25.1, 19.9, 14.2. HRMS (ESI) m/z calcd for $C_{35.5}H_{41.5}B_{0.5}N_1O_{2.5}S_1^+$ $[M/2]^+$, 559.2913; Found, 559.2922.

Preparation of dye-loaded phospholipid nanomicelles: The nanomicelles were prepared using modified film hydration technique. In a typical procedure, 100 mg of DSPE-mPEG2000 was dissolved in 0.8 mL DMF. Then 200 μL of dye solution (IRBTP-O, IRBTP-B or D632, 5 mM in DMF) was mixed. 9 mL of deionized water was added under sonication to make the clear nanomicelles solution with dye concentration of 100 μM. The nanomicelle solution was further concentrated if necessary by using a 30 K Amicon Ultra filter (Millipore Corporation) under centrifugation at 2,000 g for 5 min.

Determination of fluorescence quantum yields: Quantum yields (Φ_{fl}) were determined in various solvents relative to IR26 (Φ_{fl} = 0.05% in DCE)[36,45-49], from plots of integrated fluorescence intensity vs. absorbance, according to the following relationship:

$$\Phi_{fl,s} = \Phi_{fl,r} \times \frac{n_s^2}{n_r^2}\left(\frac{K_s}{K_r}\right) \quad (1)$$

where subscripts *r* and *s* denote standard and test sample, respectively, Φ is the fluorescence quantum yield, *K* is the slop of the integrated fluorescence intensity vs. absorbance plot, and *n* is the refractive index of the solvent. Measurements were performed with the absorbance at 808 nm of all dye solutions ≤ 0.08 in order to maximize illumination homogeneity and optical transparency. The

808 nm laser was used as the excitation source and the emission spectrum in the 900-1500 nm region was acquired in fluorescence spectrometer.

Photostability of dyes: Photostability of dyes were tested with ICG as the reference. The absorbance at max of the dye solution at the corresponding maximum absorbing wavelength was adjusted to 1 for both dyes and the reference. Both solutions were subjected to irradiation by a 2.8 W cm^{-2} 808 nm laser. The solution temperature was maintained steady by air-cooling. The absorption spectrum of the solution was checked every 30 seconds.

Determination of p*K*a values: The calculation of p*K*a values was performed with Origin 2017 software (OriginLab, Northhampton, MA), using the Bolzmman fitting function:

$$y = \frac{A_1 - A_2}{1 + e^{(x - x_0)/d_x}} + A_2 \quad (2)$$

On the basis of the calculated equation of p*K*a, x_0 corresponds to the p*K*a value.

Cell viability: $CaOV_3$ cell line was provided by American Type Culture Collection (ATCC, Manassas, VA, USA). The cytotoxicity was measured by using Cell Counting Kit-8 (CCK-8) assay. The cells (1×10^4) were incubated in each well of a 96-well plate for 24 h, then incubated with IRBTP-B and IRBTP-O micelles (dye concentration: 0, 2.5, 5, 20, 40, 50 μM) with different concentrations for 24 h, respectively. Enzyme dehydrogenase in living cells was oxidized by this kit to orange carapace. The quality was assessed calorimetrically by using a multi-reader (TECAN, Infinite M200, Germany). The measurements were based on the absorbance values at 450 nm. Following formula was used to calculate the viability of cell growth: Viability (%) = (mean absorbance value of treatment group/mean absorbance value of control group) × 100.

Animal models of drug-induced hepatotoxicity: All animal experiments were in agreement with the guidelines of Fudan University's Administrative panel on Laboratory Animal Care. Five weeks old female mice were purchased from Shanghai SLAC Laboratory animal CO. Ltd. And the animal experiments were permitted by the Shanghai Science and Technology Committee. All groups within study contained n=3 mice. Five weeks-old female nude mice (~15 g) were fasted for 12 h to avoid the possible food fluorescence interference and randomly divided into three groups: For the control group, the mice were administered an intraperitoneal injection of PBS buffer (200 μL) before being given a tail-vein injection of probe (IRBTP-B or D632, 200 μL, 1 mM. The APAP group was given an intraperitoneal injection of APAP (300 mg/kg), and then a tail-vein injection of probe (IRBTP-B or D632, 200 μL, 1 mM) 2 h later. The mice in the last group were pretreated with an intraperitoneal injection of NAC (300 mg/kg) 1 h before drug administration. Then all of the mice were anesthetized and the livers of the mouse were imaged.

Histology staining assays: Five weeks-old female nude mice (~15 g) were treated with PBS, APAP or NAC + APAP respectively following above procedure. The mice were dissected to isolate the livers, which were then fixed with 10% PFA for 48 h. Then the samples were dehydrated with ethanol and embedded in paraffin before 6 μm sectioning. H&E staining samples were prepared from the mice stained by hematoxylin and eosin under standard protocols.

RESULTS AND DISCUSSION

Design and synthesis of activatable NIR-II probe for $ONOO^-$. Polymethine dyes are one type of the widely employed fluorophores for NIR fluorescent sensor design, due to their high extinction coefficients, moderate quantum yields and facile synthesis and modification.[50-54] By introducing strong electron withdrawing groups (benzothiopyrylium) at both ends of the skeleton, a novel fluorophore is expected to emit NIR-II fluorescence (Figure 1). In addition, the turn-on fluorescence property of the fluorophore can be obtained by the fusion of a phenol moiety with methylene chain.

The incorporation of phenyl borate can actualize the responsiveness of the probe towards $ONOO^-$. When the phenol is protected by phenyl borate, the conjugated π-electron system is divided in half, which results in the masking of the NIR-II fluorescence emission. In the presence of $ONOO^-$, the dioxaborolane group is firstly oxidized to generate intermediate A, which converts to intermediate B after electron rearrangement. Further electron rearrangement results in generation of the fluorophore (IRBTP-O) with entire conjugation which is expected to emit NIR-II fluorescence. Moreover, the incorporation of various analyte triggering groups to hydroxyl should allow design of different functional NIR-II activatable probes.

Polymethine dyes are prepared through the introduction of an activated heterocycle to a bis(aldehyde) equivalent (Figure 1 and S1). Compound **1** has been synthesized by condensation of substituted 3-bromothiophenols and ethyl (4-methoxybenzoyl) acetate. The amine derivative **2** has been obtained by the Buchwald–Hartwig amination of **1** with dibutylamine. Addition of MeMgBr to the carbonyl group of **2** followed by elimination with $HClO_4$ provides the important intermediate **3**. Condensation of compound **3** with 4-hydroxy-1,3-dialdehyde or **4** yields the final pentamethine compounds IRBTP-B and IRBTP-O respectively.

Photophysical properties and penetration effect of IRBTP-O. Two absorption peaks at 575 and 905 nm are shown for IRBTP-O with its emission peak beyond 1000 nm (Figure 2a, 2b and Table S1). In comparison, IRBTP-B does not exhibit any absorption or fluorescence emission in the NIR-II region (Figure 2a and 2b). For in vivo applications, micelles containing IRBTP-O or IRBTP-B were prepared based upon prior reports with mPEG-DSPE lipids.[36] An average diameters of 8.3 and 6.3 nm, respectively, were obtained for IRBTP-O and IRBTP-B micelles (Figure S2 and S3). With IR-26 as reference (QY= 0.05 %, Table S1), the quantum yield of IRBTP-O was determined to be 0.10 % in methanol (Figure S4). Then, the absorbance and fluorescence profiles of IRBTP-O at different pH values were examined and a pKa of 6.75 was calculated from pH-fluorescence profile

(Figure S5). As can be seen, IRBTP-O shows moderate fluorescence at physiological pH, suggesting its suitability for biological applications. Compared with ICG, both IRBTP-O and IRBTP-B showed excellent photostability (Figure 2c). Next, we investigated the penetration effect of IRBTP-O in capillary tubes in different imaging windows through using long pass (LP) filters from 850 to 1300 nm on tissue phantom (1 % Intralipid in water to mimic biological soft tissue). Better resolution of the capillary tubes and attenuation of image intensities were obtained when imaging in the window with longer wavelength filters due to the reduced photon scattering (Figure 2d and S6). In addition, we also evaluated the signal-to-noise ratio (SNR) of the capillary tubes in these imaging windows. The optimal SNR was obtained at wavelength beyond 1100 nm when the covered phantom is more than 5 mm due to the much weak signal in the imaging windows beyond 1200 and 1300 nm (Figure 2e). According to the Rose criterion, it can be concluded that emissions beyond 1100 nm is favorable for in vivo applications with the relative higher SNR and higher penetration depth.

The fluorescence response of IRBTP-B towards $ONOO^-$. Next, the time dependent fluorescence response of IRBTP-B to $ONOO^-$ was studied (Figure S7), which showed the obvious enhancement of fluorescence with the time and a plateau after 3 minutes. Then, the optical sensing toward $ONOO^-$ at varied concentrations (0-11 μM) was studied in PBS buffer solutions (pH 7.4). Upon reaction with $ONOO^-$, the NIR absorption at 850 nm was generated, accompanied by the reduction of the peak at 600 nm (Figure 3a). Meanwhile, the fluorescence intensity within NIR-II window was increased gradually with increase of $ONOO^-$ concentration (Figure 3b), and a good linearity (R^2= 0.9897) was obtained with the detection limit determined to be 55.9 nM (Figure 3c). The selectivity experiment showed that biothiols (cysteine and NaHS), ROS and other RNS had no apparent influences on the fluorescence response of IRBTP-B, illustrating the good selectivity of IRBTP-B to $ONOO^-$ (Figure 3d and S8). The activatable fluorescence property of IRBTP-B was then assayed by comparison with the widely used commercial $ONOO^-$ probe D632[55] on a tissue phantom study (Figure 3e, S9 and

S10). In the absence of $ONOO^-$, both capillary tubes loading IRBTP-B and D632 showed no detectable fluorescence signals before and after being covered by Intralipid. However, when $ONOO^-$ was added, the fluorescence of IRBTP-B was turned on and the edges of the capillary tube could still be resolved from the images obtained beyond 1100 nm even at 5 mm Intralipid (Figure 3e). On the contrary, the fluorescence signal from D632 can only be detected when the thickness of Intralipid is smaller than 2 mm. In both the capillary tubes with IRBTP-B and D632 in the presence of $ONOO^-$, activated ratio decreased with increasing the thickness of Intralipid, while the line width (FWHM, full width at half maximum) showed an opposite dependence. Due to the longer emission wavelength in the NIR-II region, imaging with IRBTP-B favors more clarity than that of D632 whose emission lies in the visible region. Furthermore, the distance between the liver and skin of nude mouse is about 0.59 mm (Figure S11), which encouraged us to use IRBTP-B for *in vivo* monitoring of preclinical drug-induced hepatotoxicity. All above results indicate that IRBTP-B can be used for $ONOO^-$ detection under normal physiological conditions with deep penetration depth.

Imaging APAP-induced hepatotoxicity *in vivo.* Motivated by these promising results, we next examined the ability of IRBTP-B probe to visualize production of $ONOO^-$ in a drug-induced hepatotoxicity model in nude mice. A CCK8 assay with $CaOV_3$ cells was first performed and identified the low cytotoxicity of IRBTP-B and IRBTP-O (Figure S12). It is well-known that an overdose of APAP, a commonly household antipyretic and analgesic agent, is the leading cause of hepatotoxicity even acute liver failure due to the overproduction of RNS. Therefore, by guiding with the imaging biomarker $ONOO^-$, drug-induced liver damage can be visualized in nude mice with the aid of IRBTP-B. Meanwhile, N-acetyl cysteine (NAC) was used as the antidote for APAP overdose, which was reported to remediate cell injury via the depletion of the RNS levels by increasing the GSH level and binding with the toxic metabolite of APAP. Generally, female nude mice were randomly divided into three groups: PBS (control group), APAP, and NAC + APAP. 300 mg kg^{-1} of

APAP and 300 mg kg^{-1} of NAC were Intraperitoneal injected as needed because those doses are reported to efficiently induce and recover inflammation respectively.[17] Weak fluorescence signal was obtained in the mice liver of the control group, implying little production of $ONOO^-$ level under normal conditions (Figure 4a). In contrast, after the administration of APAP, the fluorescence intensities of the mice livers displayed gradual increments in a time-dependent manner and reached a maximum after 15 minutes of injection of IRBTP-B (Figure 4a and 4b), indicating the increased generation of $ONOO^-$ after drug treatment. Moreover, no obvious fluorescent intensity augmentation was observed with time in the NAC pretreatment group, indicating effective NAC remediation. Similar procedures were also performed to evaluate commercial $ONOO^-$ probe D632 (Figure 4c and S13). In comparison, higher SNR and relative fluorescent intensity were obtained from IRBTP-B due to the reduced autofluorescence and photon scattering in NIR-II window (Figure 4d and 4e), indicating IRBTP-B is more sensitive than commercial D632 for *in vivo* imaging. Next, the histological analysis on the liver tissues were carried out to identify the histological changes during the drug administration (Figure 4f). The livers from the control group were found to have intact centrilobular vein (arrow 1), healthy hepatocytes and liver cells were arranged in the radial shape with the center of central vein. On the contrary, a non-uniform morphology of the hepatocytes, inflammatory cells infiltration (arrow 2), and hemorrhage (arrow 3) could be obviously observed after the administration of APAP, implying APAP-induced liver injury. Significantly improved symptoms could be observed with NAC pretreatment, indicating effective remediation with NAC. These results were in good agreement with the observation of in vivo fluorescence imaging.

CONCLUSION

In summary, we have constructed an $ONOO^-$ activatable NIR-II probe for APAP-induced hepatotoxicity monitoring. It was found that an apparent $ONOO^-$ level upregulation occurred during the drug-induced liver damage. Therefore, we anticipate that IRBTP-B may be employed as a

powerful tool to probe $ONOO^-$ for preclinical drug-induced organism injury. Preclinical interrogation of drug hepatotoxicity will add benefits in improving patient safety and therapeutic outcomes. We expect that this strategy may be extended for the development of a wide variety of activatable NIR-II probes by masking the hydroxyl functionalized reactive site with an analyte-specific triggering group.

ASSOCIATED CONTENT

Supporting Information paragraph.

Experimental section and additional information as noted in the text. This material is available free of charge *via* the Internet at http://pubs.acs.org.

AUTHOR INFORMATION

Corresponding Author

E-mail: zhang_fan@fudan.edu.cn.

Tel: (+86)21-51630322; Fax: (+86)21-5163-0307.

Notes

The authors declare no competing financial interest.

ACKNOWLEDGMENT

The work was supported by the National Key R & D Program of China (2017YFA0207303), National Science Fund for Distinguished Young Scholars (21725502), Key Basic Research Program of Science and Technology Commission of Shanghai Municipality (17JC1400100), and China Postdoctoral Science Foundation (Grant KLH1615151). The authors extend their appreciation to the

International Scientific Partnership Program ISPP at King Saud University for funding this research work through ISPP#0100.

REFERENCES

(1) Liebler, D. C.; Guengerich, F. P., Elucidating Mechanisms of Drug-Induced Toxicity. *Nat. Rev. Drug Discov.* **2005,** *4*, 410-420.
(2) Park, B. K.; Kitteringham, N. R.; Maggs, J. L.; Pirmohamed, M.; Williams, D. P., The Role of Metabolic Activation in Drug-Induced Hepatotoxicity. *Annu. Rev. Pharmacol. Toxicol.* **2005,** *45*, 177-202.
(3) Lee, W. M., Drug-Induced Hepatotoxicity. *New Engl. J. Med.* **2003,** *349*, 474-485.
(4) Stefan, R.; Gerd, A. K.-U.; Ignazio, G., Current Concepts of Mechanisms in Drug-Induced Hepatotoxicity. *Curr. Med. Chem.* **2009,** *16*, 3041-3053.
(5) Walsh, J. S.; Miwa, G. T., Bioactivation of Drugs: Risk and Drug Design. *Annu. Rev. Pharmacol. Toxicol.* **2011,** *51*, 145-167.
(6) Schäferling, M., The Art of Fluorescence Imaging with Chemical Sensors. *Angew. Chem. Int. Ed.* **2012,** *51*, 3532-3554.
(7) Gorris, H. H.; Wolfbeis, O. S., Photon-Upconverting Nanoparticles for Optical Encoding and Multiplexing of Cells, Biomolecules, and Microspheres. *Angew. Chem. Int. Ed.* **2013,** *52*, 3584-3600.
(8) Han, M.; Gao, X.; Su, J. Z.; Nie, S., Quantum-Dot-Tagged Microbeads for Multiplexed Optical Coding of Biomolecules. *Nat. Biotechnol.* **2001,** *19*, 631-635.
(9) Liu, B.; Li, C.; Yang, P.; Hou, Z.; Lin, J., 808-nm-Light-Excited Lanthanide-Doped Nanoparticles: Rational Design, Luminescence Control and Theranostic Applications. *Adv. Mater.* **2017,** *29*, 1605434.
(10) Li, Y.; Xie, X.; Yang, X. e.; Li, M.; Jiao, X.; Sun, Y.; Wang, X.; Tang, B., Two-Photon Fluorescent Probe for Revealing Drug-Induced Hepatotoxicity via Mapping Fluctuation of Peroxynitrite. *Chem. Sci.* **2017,** *8*, 4006-4011.
(11) Jia, X.; Chen, Q.; Yang, Y.; Tang, Y.; Wang, R.; Xu, Y.; Zhu, W.; Qian, X., FRET-Based Mito-Specific Fluorescent Probe for Ratiometric Detection and Imaging of Endogenous Peroxynitrite: Dyad of Cy3 and Cy5. *J. Am. Chem. Soc.* **2016,** *138*, 10778-10781.
(12) He, X.; Li, L.; Fang, Y.; Shi, W.; Li, X.; Ma, H., In Vivo Imaging of Leucine Aminopeptidase Activity in Drug-Induced Liver Injury and Liver Cancer via a Near-Infrared Fluorescent Probe. *Chem. Sci.* **2017,** *8*, 3479-3483.
(13) Cheng, D.; Xu, W.; Yuan, L.; Zhang, X., Investigation of Drug-Induced Hepatotoxicity and Its Remediation Pathway with Reaction-Based Fluorescent Probes. *Anal. Chem.* **2017,** *89*, 7693-7700.
(14) Peng, J.; Samanta, A.; Zeng, X.; Han, S.; Wang, L.; Su, D.; Loong, D. T. B.; Kang, N. Y.; Park, S. J.; All, A. H.; Jiang, W.; Yuan, L.; Liu, X.; Chang, Y. T., Real-Time In Vivo Hepatotoxicity Monitoring through Chromophore-Conjugated Photon-Upconverting Nanoprobes. *Angew. Chem. Int. Ed.* **2017,** *56*, 4165-4169.
(15) Zhang, Q.; Zhu, Z.; Zheng, Y.; Cheng, J.; Zhang, N.; Long, Y.-T.; Zheng, J.; Qian, X.; Yang, Y., A Three-Channel Fluorescent Probe That Distinguishes Peroxynitrite from Hypochlorite. *J. Am. Chem. Soc.* **2012,** *134*, 18479-18482.

(16) Song, Z.; Mao, D.; Sung, S. H. P.; Kwok, R. T. K.; Lam, J. W. Y.; Kong, D.; Ding, D.; Tang, B. Z., Activatable Fluorescent Nanoprobe with Aggregation-Induced Emission Characteristics for Selective In Vivo Imaging of Elevated Peroxynitrite Generation. *Adv. Mater.* **2016,** *28*, 7249-7256.
(17) Shuhendler, A. J.; Pu, K.; Cui, L.; Uetrecht, J. P.; Rao, J., Real-Time Imaging of Oxidative and Nitrosative Stress in the Liver of Live Animals for Drug-Toxicity Testing. *Nat. Biotechnol.* **2014,** *32*, 373.
(18) Oushiki, D.; Kojima, H.; Terai, T.; Arita, M.; Hanaoka, K.; Urano, Y.; Nagano, T., Development and Application of a Near-Infrared Fluorescence Probe for Oxidative Stress Based on Differential Reactivity of Linked Cyanine Dyes. *J. Am. Chem. Soc.* **2010,** *132*, 2795-2801.
(19) Kojima, R.; Takakura, H.; Kamiya, M.; Kobayashi, E.; Komatsu, T.; Ueno, T.; Terai, T.; Hanaoka, K.; Nagano, T.; Urano, Y., Development of a Sensitive Bioluminogenic Probe for Imaging Highly Reactive Oxygen Species in Living Rats. *Angew. Chem. Int. Ed.* **2015,** *54*, 14768-14771.
(20) Yang, D.; Wang, H.-L.; Sun, Z.-N.; Chung, N.-W.; Shen, J.-G., A Highly Selective Fluorescent Probe for the Detection and Imaging of Peroxynitrite in Living Cells. *J. Am. Chem. Soc.* **2006,** *128*, 6004-6005.
(21) Liu, D.; Feng, S.; Feng, G., A Rapid Responsive Colorimetric and Near-Infrared Fluorescent Turn-On Probe for Imaging Exogenous and Endogenous Peroxynitrite in Living Cells. *Sens. Actuators B* **2018,** *269*, 15-21.
(22) Feng, S.; Liu, D.; Feng, G., A Dual-Channel Probe with Green and Near-Infrared Fluorescence Changes for In Vitro and In Vivo Detection of Peroxynitrite. *Anal. Chim. Acta* **2019,** *1054*, 137-144.
(23) Feng, W.; Feng, G., A Lysosome-Targetable Fluorescent Probe for Imaging $ONOO^-$ in Living Cells and Animals. *Dyes Pigm.* **2019,** *164*, 174-181.
(24) Cheng, D.; Pan, Y.; Wang, L.; Zeng, Z.; Yuan, L.; Zhang, X.; Chang, Y.-T., Selective Visualization of the Endogenous Peroxynitrite in an Inflamed Mouse Model by a Mitochondria-Targetable Two-Photon Ratiometric Fluorescent Probe. *J. Am. Chem. Soc.* **2017,** *139*, 285-292.
(25) Li, H.; Li, X.; Wu, X.; Shi, W.; Ma, H., Observation of the Generation of $ONOO^-$ in Mitochondria under Various Stimuli with a Sensitive Fluorescence Probe. *Anal. Chem.* **2017,** *89*, 5519-5525.
(26) Ntziachristos, V.; Ripoll, J.; Wang, L. V.; Weissleder, R., Looking and Listening to Light: The Evolution of Whole-Body Photonic Imaging. *Nat. Biotechnol.* **2005,** *23*, 313-320.
(27) Hong, G.; Antaris, A. L.; Dai, H., Near-Infrared Fluorophores for Biomedical Imaging. *Nat. Biomed. Eng.* **2017,** *1*, 0010.
(28) Smith, A. M.; Mancini, M. C.; Nie, S., Second Window for In Vivo Imaging. *Nat. Nanotechnol.* **2009,** *4*, 710-711.
(29) He, S.; Song, J.; Qu, J.; Cheng, Z., Crucial Breakthrough of Second Near-Infrared Biological Window Fluorophores: Design and Synthesis toward Multimodal Imaging and Theranostics. *Chem. Soc. Rev.* **2018,** *47*, 4258-4278.
(30) Schnermann, M. J., Organic Dyes for Deep Bioimaging. *Nature* **2017,** *551*, 176.
(31) Yomogida, Y.; Tanaka, T.; Zhang, M.; Yudasaka, M.; Wei, X.; Kataura, H., Industrial-Scale Separation of High-Purity Single-Chirality Single-Wall Carbon Nanotubes for Biological Imaging. *Nat. Commun.* **2016,** *7*, 12056.
(32) Bruns, O. T.; Bischof, T. S.; Harris, D. K.; Franke, D.; Shi, Y.; Riedemann, L.; Bartelt, A.; Jaworski, F. B.; Carr, J. A.; Rowlands, C. J.; Wilson, M. W. B.; Chen, O.; Wei, H.; Hwang, G. W.; Montana, D. M.; Coropceanu, I.; Achorn, O. B.; Kloepper, J.; Heeren, J.; So, P. T. C.; Fukumura, D.; Jensen, K. F.; Jain, R. K.; Bawendi, M. G., Next-Generation In Vivo Optical Imaging with Short-Wave Infrared Quantum Dots. *Nat. Biomed. Eng.* **2017,** *1*, 0056.

(33) Fan, Y.; Wang, P.; Lu, Y.; Wang, R.; Zhou, L.; Zheng, X.; Li, X.; Piper, J. A.; Zhang, F., Lifetime-Engineered NIR-II Nanoparticles Unlock Multiplexed In Vivo Imaging. *Nat. Nanotechnol.* **2018,** *13*, 941-946.
(34) Zhong, Y.; Ma, Z.; Zhu, S.; Yue, J.; Zhang, M.; Antaris, A. L.; Yuan, J.; Cui, R.; Wan, H.; Zhou, Y.; Wang, W.; Huang, N. F.; Luo, J.; Hu, Z.; Dai, H., Boosting the Down-Shifting Luminescence of Rare-Earth Nanocrystals for Biological Imaging beyond 1500 nm. *Nat. Commun.* **2017,** *8*, 737.
(35) Antaris, A. L.; Chen, H.; Cheng, K.; Sun, Y.; Hong, G.; Qu, C.; Diao, S.; Deng, Z.; Hu, X.; Zhang, B.; Zhang, X.; Yaghi, O. K.; Alamparambil, Z. R.; Hong, X.; Cheng, Z.; Dai, H., A Small-Molecule Dye for NIR-II Imaging. *Nat. Mater.* **2016,** *15*, 235-242.
(36) Cosco, E. D.; Caram, J. R.; Bruns, O. T.; Franke, D.; Day, R. A.; Farr, E. P.; Bawendi, M. G.; Sletten, E. M., Flavylium Polymethine Fluorophores for Imaging in the Near- and Shortwave Infrared. *Angew. Chem. Int. Ed.* **2017,** *56*, 13126-13129.
(37) Li, B.; Lu, L.; Zhao, M.; Lei, Z.; Zhang, F., An Efficient 1064 nm NIR-II Excitation Fluorescent Molecular Dye for Deep-Tissue High-Resolution Dynamic Bioimaging. *Angew. Chem. Int. Ed.* **2018,** *57*, 7483-7487.
(38) Sheng, Z.; Guo, B.; Hu, D.; Xu, S.; Wu, W.; Liew, W. H.; Yao, K.; Jiang, J.; Liu, C.; Zheng, H.; Liu, B., Bright Aggregation-Induced-Emission Dots for Targeted Synergetic NIR-II Fluorescence and NIR-I Photoacoustic Imaging of Orthotopic Brain Tumors. *Adv. Mater.* **2018,** *30*, 1800766, https://doi.org/10.1002/adma.201800766.
(39) Wan, H.; Yue, J.; Zhu, S.; Uno, T.; Zhang, X.; Yang, Q.; Yu, K.; Hong, G.; Wang, J.; Li, L.; Ma, Z.; Gao, H.; Zhong, Y.; Su, J.; Antaris, A. L.; Xia, Y.; Luo, J.; Liang, Y.; Dai, H., A Bright Organic NIR-II Nanofluorophore for Three-Dimensional Imaging into Biological Tissues. *Nat. Commun.* **2018,** *9*, 1171.
(40) Ding, F.; Zhan, Y.; Lu, X.; Sun, Y., Recent Advances in Near-Infrared II Fluorophores for Multifunctional Biomedical Imaging. *Chem. Sci.* **2018,** *9*, 4370-4380.
(41) Tao, Z.; Hong, G.; Shinji, C.; Chen, C.; Diao, S.; Antaris, A. L.; Zhang, B.; Zou, Y.; Dai, H., Biological Imaging Using Nanoparticles of Small Organic Molecules with Fluorescence Emission at Wavelengths Longer than 1000 nm. *Angew. Chem. Int. Ed.* **2013,** *125*, 13240-13244.
(42) Shou, K.; Qu, C.; Sun, Y.; Chen, H.; Chen, S.; Zhang, L.; Xu, H.; Hong, X.; Yu, A.; Cheng, Z., Multifunctional Biomedical Imaging in Physiological and Pathological Conditions Using a NIR-II Probe. *Adv. Funct. Mater.* **2017,** *27*, 1700995.
(43) Hori, Y.; Nakaki, K.; Sato, M.; Mizukami, S.; Kikuchi, K., Development of Protein-Labeling Probes with a Redesigned Fluorogenic Switch Based on Intramolecular Association for No-Wash Live-Cell Imaging. *Angew. Chem. Int. Ed.* **2012,** *51*, 5611-5614.
(44) Xu, G.; Yan, Q.; Lv, X.; Zhu, Y.; Xin, K.; Shi, B.; Wang, R.; Chen, J.; Guo, W.; Shi, P.; Fan, C.; Zhao, C.; Tian, H., Imaging of Colorectal Cancers Using Activatable Nanoprobes with Second Near-Infrared Window Emission. *Angew. Chem. Int. Ed.* **2018,** *57*, 3626-3630.
(45) Lin, Q. L.; Yun, H. J.; Liu, W. Y.; Song, H. J.; Makarov, N. S.; Isaienko, O.; Nakotte, T.; Chen, G.; Luo, H. M.; Klimov, V. I.; Pietryga, J. M., Phase-Transfer Ligand Exchange of Lead Chalcogenide Quantum Dots for Direct Deposition of Thick, Highly Conductive Films. *J. Am. Chem. Soc.* **2017,** *139*, 6644-6653.
(46) Reineck, P.; Gibson, B. C., Near-Infrared Fluorescent Nanomaterials for Bioimaging and Sensing. *Adv. Optical Mater.* **2017,** *5*, 1600446.
(47) Sun, Y.; Ding, F.; Zhou, Z.; Li, C.; Pu, M.; Xu, Y.; Zhan, Y.; Lu, X.; Li, H.; Yang, G.; Sun, Y.; Stang, P. J., Rhomboidal Pt(II) metallacycle-based NIR-II theranostic nanoprobe for tumor diagnosis and image-guided therapy. *Proc. Natl. Acad. Sci. USA* **2019,** *116*, 1968-1973.

(48) Zhu, S.; Yung, B. C.; Chandra, S.; Niu, G.; Antaris, A. L.; Chen, X., Near-Infrared-II (NIR-II) Bioimaging via Off-Peak NIR-I Fluorescence Emission. *Theranostics* **2018,** *8*, 4141-4151.
(49) Semonin, O. E.; Johnson, J. C.; Luther, J. M.; Midgett, A. G.; Nozik, A. J.; Beard, M. C., Absolute Photoluminescence Quantum Yields of IR-26 Dye, PbS, and PbSe Quantum Dots. *J. Phys. Chem. Lett.* **2010,** *1*, 2445-2450.
(50) Hyun, H.; Wada, H.; Bao, K.; Gravier, J.; Yadav, Y.; Laramie, M.; Henary, M.; Frangioni, J. V.; Choi, H. S., Phosphonated Near-Infrared Fluorophores for Biomedical Imaging of Bone. *Angew. Chem. Int. Ed.* **2014,** *53*, 10668-10672.
(51) Carr, J. A.; Franke, D.; Caram, J. R.; Perkinson, C. F.; Saif, M.; Askoxylakis, V.; Datta, M.; Fukumura, D.; Jain, R. K.; Bawendi, M. G.; Bruns, O. T., Shortwave Infrared Fluorescence Imaging with the Clinically Approved Near-Infrared Dye Indocyanine Green. *Proc. Natl. Acad. Sci. USA* **2018,** *115*, 4465-4470.
(52) Yin, J.; Kwon, Y.; Kim, D.; Lee, D.; Kim, G.; Hu, Y.; Ryu, J.-H.; Yoon, J., Cyanine-Based Fluorescent Probe for Highly Selective Detection of Glutathione in Cell Cultures and Live Mouse Tissues. *J. Am. Chem. Soc.* **2014,** *136*, 5351-8.
(53) Karton-Lifshin, N.; Albertazzi, L.; Bendikov, M.; Baran, P. S.; Shabat, D., "Donor-Two-Acceptor" Dye Design: A Distinct Gateway to NIR Fluorescence. *J. Am. Chem. Soc.* **2012,** *134*, 20412-20420.
(54) Li, H.; Li, X.; Shi, W.; Xu, Y.; Ma, H., Rationally Designed Fluorescence ·OH Probe with High Sensitivity and Selectivity for Monitoring the Generation of ·OH in Iron Autoxidation without Addition of H_2O_2. *Angew. Chem. Int. Ed.* **2018,** *57*, 12830-12834.
(55) Szabó, C.; Virág, L.; Cuzzocrea, S.; Scott, G. S.; Hake, P.; O'Connor, M. P.; Zingarelli, B.; Salzman, A.; Kun, E., Protection Against Peroxynitrite-Induced Fibroblast Injury and Arthritis Development by Inhibition of Poly(ADP-ribose) Synthase. *Proc. Natl. Acad. Sci. USA* **1998,** *95*, 3867-3872.

FIGURE CAPTION

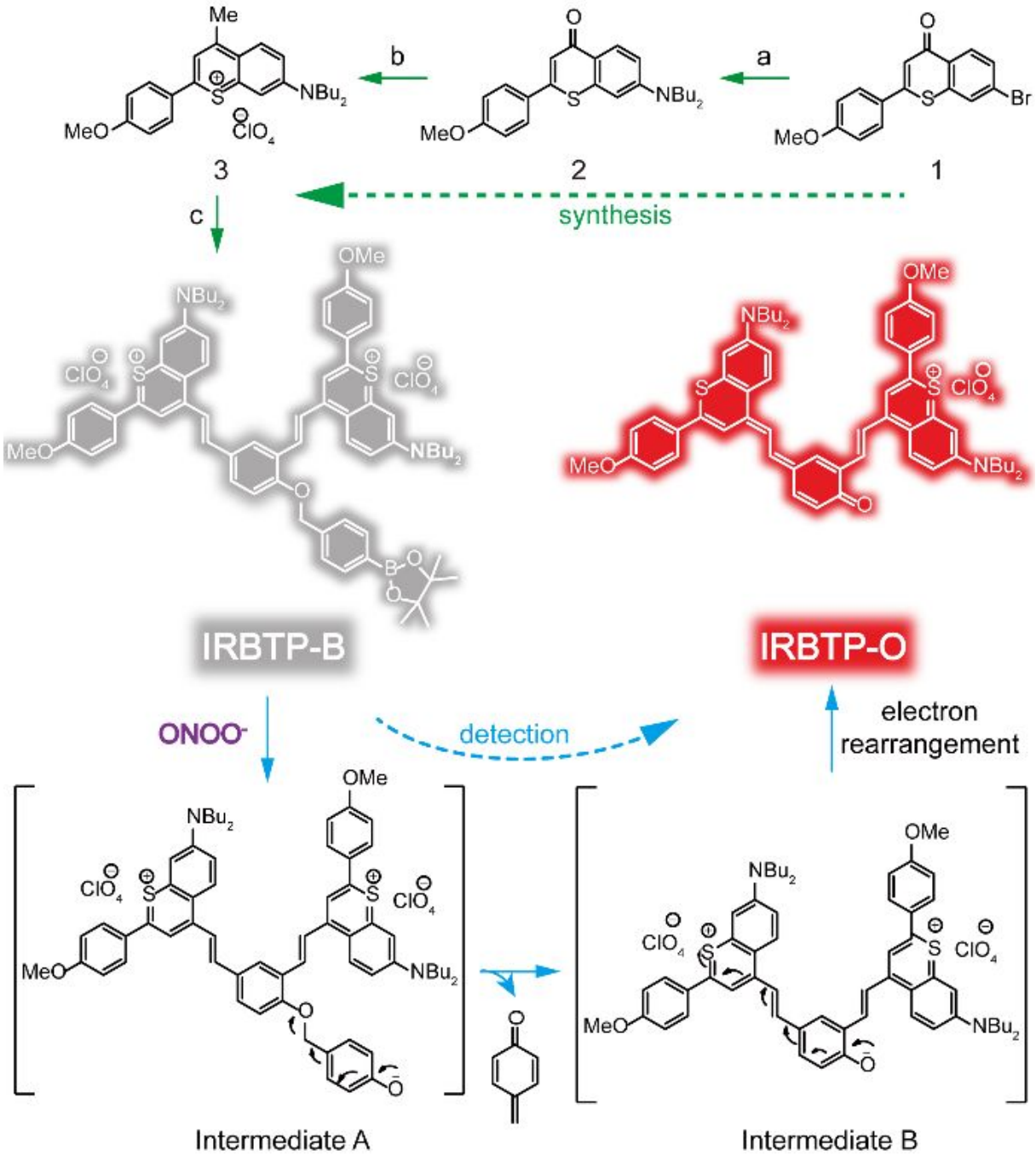

Figure 1. Design and synthesis of $ONOO^-$ activatable molecular probe with NIR-II fluorescence. Conditions: a) Et_2NH, $Pd_2(dba)_3$, DavePhos, Cs_2CO_3, dioxene, 95 °C, 18h; b) i CH_3MgBr, ii $HClO_4$; c) toluene/n-butanol, 100 °C, 12h.

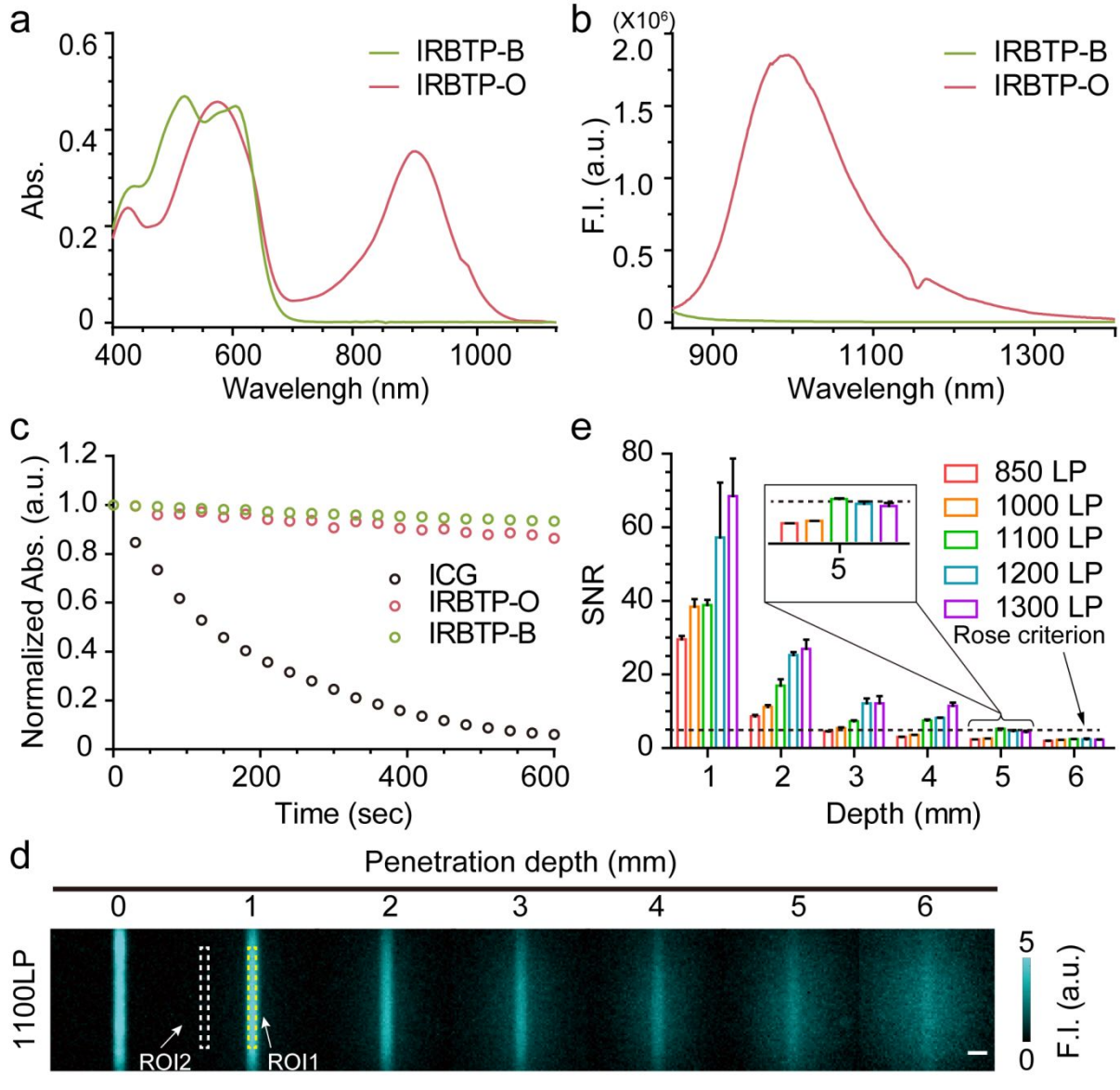

Figure 2. (a) Absorption and (b) fluorescence of IRBTP-O and IRBTP-B in $CHCl_3$. (c) Photostability comparison of ICG, IRBTP-B and IRBTP-O in PBS. (d) Fluorescence images of capillaries filled with IRBTP-O in NIR-II (1100 nm LP) region immersed in 1% Intralipid with varying depth, Scale bar: 2 mm. (e) Measured SNR of capillary images under different depth. SNR values were calculated by dividing average signal intensity (ROI1) by the average back-ground signal intensity (ROI2). Insert: SNR of capillary images under 5 mm.

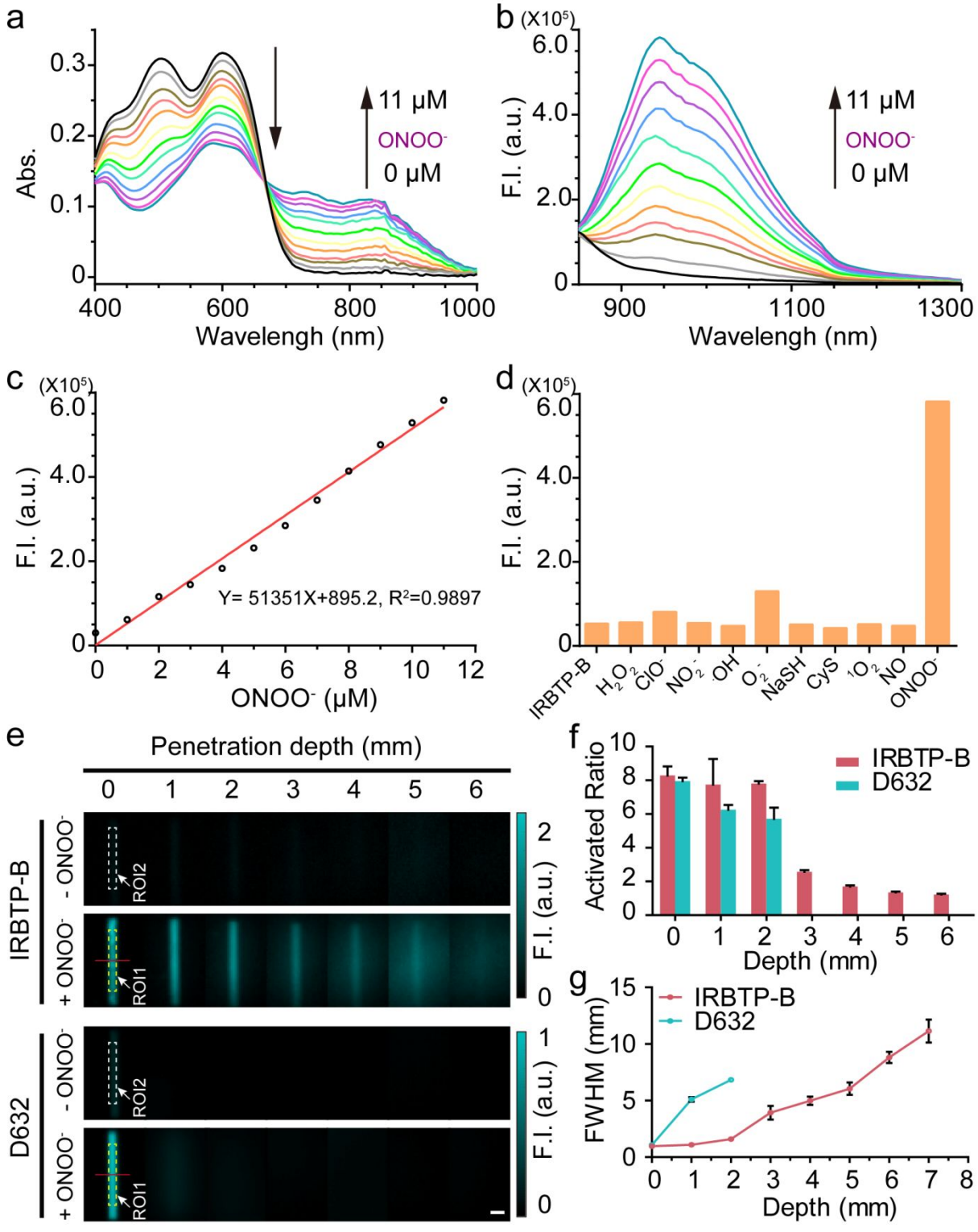

Figure 3. (a) Absorption and (b) fluorescence changes of IRBTP-B (10 μM) upon addition with $ONOO^-$ (0 - 11 μM) in PBS. (c) Plots of fluorescence intensity at 950 nm with varied concentrations

of $ONOO^-$ in PBS. (d) The fluorescent response of IRBTP-B to bioreactive reagents. (e) Tissue phantom study of the penetration depth of IRBTP-B (1100 nm LP) and D632 (540 nm band pass (BP)) in the absence and presence of $ONOO^-$. (f) Activated ratio comparison of IRBTP-B and D632 under different depth. Activated ratio values were calculated by dividing average signal intensity of ROI1 by the average signal intensity of ROI2. (g) Feature width of capillary images filled with IRBTP-B or D632 in the presence of $ONOO^-$ as a function of depth in 1% Intralipid.

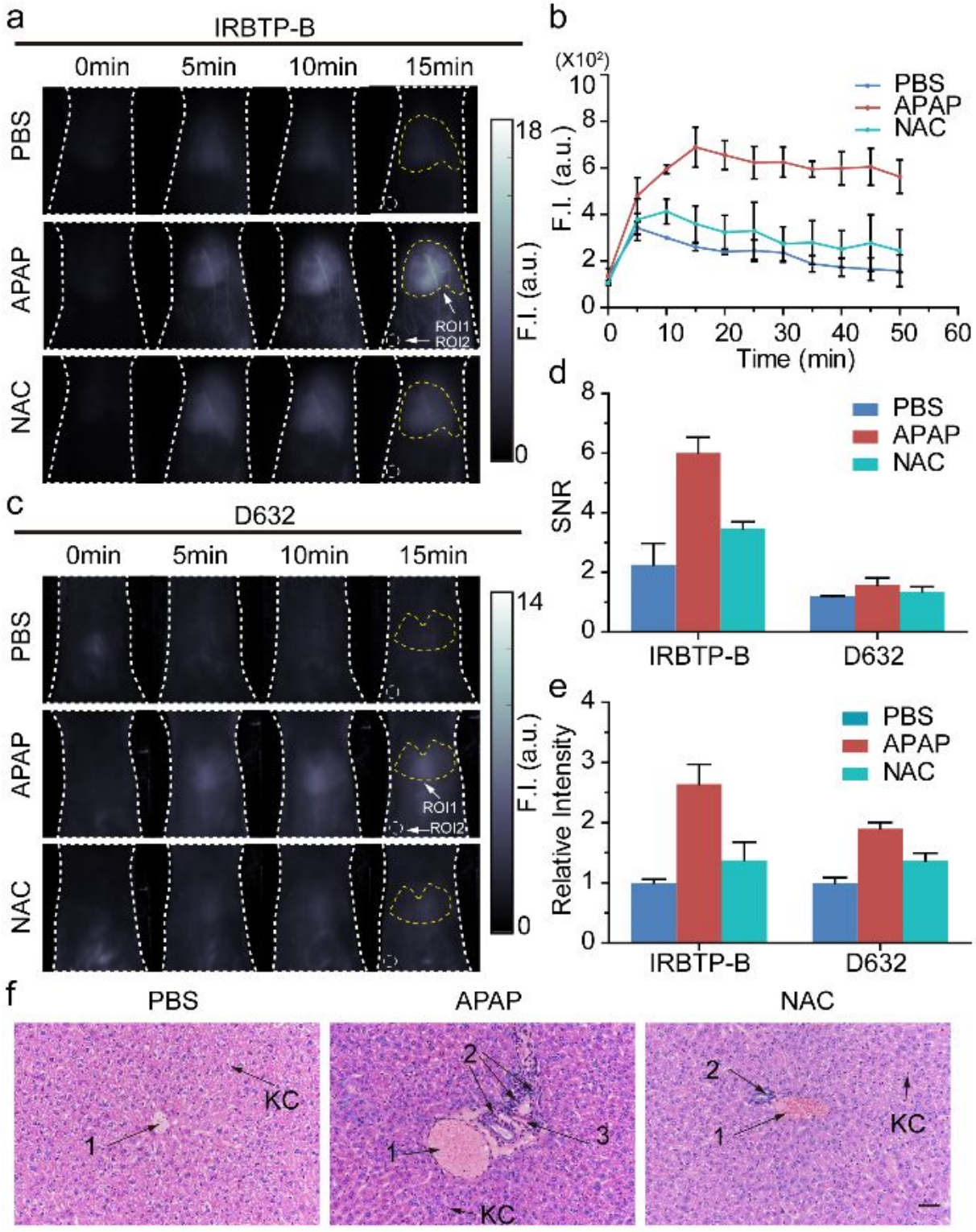

Figure 4. In vivo imaging of endogenous $ONOO^-$ in the livers of mice during an APAP-induced hepatotoxicity by IRBTP-B and D632. (a) In vivo imaging of livers of mice from IRBTP-B treated

with various substances: PBS, APAP, and NAC + APAP. (b) Relative fluorescence intensity of livers of mice treated with various substances following by IRBTP-B over time. (c) In vivo imaging of livers of mice from D632 treated with various substances: PBS, APAP, and NAC + APAP. (d) Signal to noise ratios (SNR) obtained for IRBTP-B and D632 from different groups. (e) Relative intensity of livers of mice after injection of IRBTP-B and D632 in different groups. (f) Representative histology (hematoxylin and eosin staining (H&E)) of the livers of mice treated with PBS, APAP or NAC + APAP (arrow 1: centrilobular vein, arrow 2: inflammatory cells infiltration, arrow 3: hemorrhage, KC: Kupffer cell.) Scal bar: 50 μm.

For TOC only

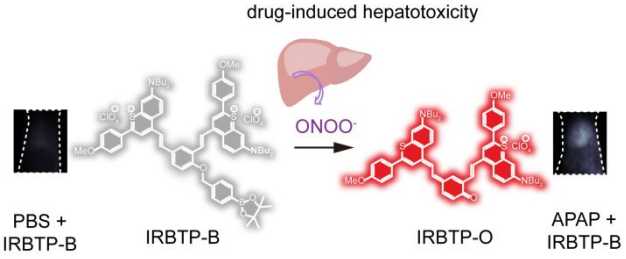
drug-induced hepatotoxicity
ONOO-
PBS +
IRBTP-B
IRBTP-B
IRBTP-O
APAP +
IRBTP-B